Surfaces and Interfaces 41 (2023) 103182

Contents lists available at ScienceDirect

Surfaces and Interfaces

journal homepage: www.sciencedirect.com/journal/surfaces-and-interfaces

The role of interfaces and morphology on silver diffusion in hard coatings

D. Cavaleiro [a,*], F. Munnik [b], M. Krause [b], E. Carbo-Argibay [c], P.J. Ferreira [c,d,e], A. Cavaleiro [a,f], F. Fernandes [a,g,*]

[a] University of Coimbra, CEMMPRE, ARISE, Department of Mechanical Engineering, Rua Luís Reis Santos, 3030-788 Coimbra, Portugal
[b] Helmholtz-Zentrum Dresden-Rossendorf, Bautzner Landstrasse 400, Dresden 01328, Germany
[c] INL – International Iberian Nanotechnology Laboratory, Av. Mestre José Veiga s/n, Braga 4715-330, Portugal
[d] Mechanical Engineering Department and IDMEC, Instituto Superior Técnico, University of Lisbon, Av. Rovisco Pais, Lisboa 1049-001, Portugal
[e] Materials Science and Engineering Program, the University of Texas at Austin, Austin, TX 78712, United States
[f] Laboratório de Ensaios, Desgaste e Materiais, IPN - LED&MAT - Instituto Pedro Nunes, Rua Pedro Nunes, Coimbra 3030-199, Portugal
[g] ISEP, Polytechnic of Porto, Rua Dr. António Bernardino de Almeida, 4249-015 Porto, Portugal

ARTICLE INFO

Keywords:
TiN and TiSiN layer stacks
Ag diffusion, Structure
Morphology

ABSTRACT

One of the main approaches to increase the tool lifetime during dry machining of "hard-to-machine" aerospace alloys is self-lubrication by the incorporation of noble metals in hard matrixes with good mechanical and diffusion barrier properties. In this paper, the diffusion of an Ag-rich layer sandwiched between two layers of either TiN or TiSiN is studied by transmission electron microscopy and *in situ* Rutherford backscattering spectrometry. The layer stacks were subjected to annealing treatments at 600 °C and 800 °C for 2 hours. Three processes were found to control the diffusion of silver: the morphology of the "sandwich" layers, the formation of small voids in the involved interfaces and the sublimation of Ag in the surface at temperatures near the melting point. The study revealed that the dense TiSiN matrix allowed a significantly better control of Ag diffusion than the more open TiN matrix.

1. Introduction

The process of machining has a significant impact in the environment as it currently consumes significant natural resources and energy [1,2]. In particular, machining intends to give a final shape to a part, concomitant with certain surface properties and dimensional accuracy, thus requiring a large amount of power [3,4]. Recently, the subject of *dry machining* (without the use of liquid lubricants or cooling) has been the focus of many publications, as it provides a major step towards a more sustainable process [5]. In fact, this technology has become increasingly popular for the automotive and aerospace industries, where "hard-to-machine" metal alloys are used to produce lightweight and structural components and airframes [6,7]. In this case, the machining conditions generated during processing lead to extremely high temperatures and shear stresses that reduce tool lifetime thus, diminishing the production rate and increasing costs [8–10].

The most promising way of extending the service lifetime of cutting tools used in the aforementioned industries is through the application of coatings that can help protect and enhance their surface properties [10–13]. In this regard, the so-called self-lubricant coatings are particularly attractive. They make use of solid-lubrication based on self-adaptive mechanisms, which due to its own intrinsic properties and/or when combined with other elements can lead to the formation of a protective tribolayer, effectively reducing the friction and temperature in the contact zone [14,15]. The mechanisms associated with solid lubrication are typically linked with different types of chemical elements, namely 1) basal plane formation and Transition Metal Dichalcogenides (TMD's) [16–19]; 2) lubricious oxide formation and Magnéli oxide phases [20–22] and 3) noble metal diffusion, such as gold or silver [23–25]. Amongst these mechanisms, noble metal diffusion is the most promising for machining of "hard-to-machine" alloys.

Silver is as a reliable noble metal to be used in solid lubrication due to its low shear strength over a wide range of temperatures, while having a relatively high melting point [26] and an extensive array of well-known functional mechanical, tribological, biological and optical properties [27]. In particular, its residual stresses (that helps increasing adhesion properties) [28], hardness (which inhibits plastic deformation) [29] and the friction coefficient [30,31] (reducing temperature and stresses generated) are all important parameters to consider when contemplating coatings to be applied in the machining process. When applied as

* Corresponding authors at: University of Coimbra, CEMMPRE, ARISE, Department of Mechanical Engineering, Rua Luís Reis Santos, 3030-788 Coimbra, Portugal
E-mail addresses: diogo.cavaleiro@dem.uc.pt (D. Cavaleiro), fid@isep.ipp.pt (F. Fernandes).

https://doi.org/10.1016/j.surfin.2023.103182
Received 19 April 2023; Received in revised form 6 July 2023; Accepted 13 July 2023
Available online 14 July 2023

solid lubricant in a hard ceramic matrix, silver may diffuse to the surface and work as a lubricant agent in the contact zone. This was first reported for YSZ-Ag adaptive coatings, where migration and coalescence of silver to the surface was induced in wear tests by sliding in air at 500 °C [32]. In this case, the friction coefficient was reduced and the wear resistance of films was improved. Yet, these benefits were not lasting, as a rapid release of Ag was observed, followed by a fast depletion of Ag from the entire volume of the coating, leading to a swift loss of the low-friction tribolayer [33].

Currently, this challenge for self-lubricant coatings remains, i.e., to be able to control the diffusion rate of the lubricious element, in order to obtain long-term low friction and higher wear resistance [15]. The most promising approach to address this challenge has been the use of diffusion barrier layers, such as TiN or CrN cap layers deposited on top of self-lubricant coatings [34,35]. Yet, those proved to be of short-term efficiency. Another innovative approach has been the encapsulation of a lubricious element in a dense barrier layer, using a material with excellent thermal and chemical stability at elevated temperatures, as well as high mechanical strength and toughness. This would help with long-term control of diffusion. The nanocomposite TiSiN coating (nc-TiN/a-SiN_x) has proven to successfully exhibit those properties [36], if combined with an efficient barrier, such as an amorphous SiN phase [37]. More recently, Cavaleiro et. al. [38,39] successfully showed that TiSiN can be a successful candidate to halt the long-term diffusion of silver, while improving the tool lifetime during the dry turning of "hard-to-machine" titanium alloys [40].

In this context, this work focuses on monitoring the diffusion of silver, through two different well-known hard matrixes (TiN and TiSiN), by Transmission Electron Microscopy (TEM) and Rutherford Backscattering Spectrometry (RBS), to assess the diffusion rates and elemental distribution after the annealing treatment. This will allow us to understand the effect of the microstructure of hard coatings on the diffusion behaviour of silver. This may confirm the potential of these coatings in cutting tools, especially for "hard-to-machine" aerospace alloys.

2. Experimental procedure

Two types of layer stacks were deposited and studied in this work, involving a fixed "central" layer of TiN doped with Ag, bounded by two different types of outer layers (TiN or TiSiN), which sandwich the central layer (Fig. 1). The thickness of the "central" layer is approximately 50 nm, whilst both the TiN and the TiSiN outer layers have approximately 100 nm in thickness. Later, a 150 nm Si_3N_4 cap layer was deposited on top of some of the layer stacks.

The TiN layers were deposited by HiPIMS (high power impulse magnetron sputtering) working in DOMS mode (deep oscillation magnetron sputtering) using a pure titanium target (99.9 %). The average power applied to the target was 1200 W. A nitrogen (N_2) partial pressure of 0.27 Pa and argon partial pressure of 0.43 Pa were used, resulting in a final deposition pressure of 0.7 Pa. As for the deposition of the TiSiN layers, a titanium target with Si pellets was used and connected to the HiPIMS power supply, using the same deposition parameters as for the TiN layers. The HiPIMS pulse used for the aforementioned cases was also used for both the layer stacks (charging voltage at the capacitors of DC340, constant on time t_{on} of 6 μs, an oscillation period of 80 μs and a pulse duration of 1500 μs). A more detailed description of the procedure can be found in our previous work [38]. For the deposition of the "central" layer, common to both films, a pure titanium target (99.9%) drilled with 20 holes of 10 mm diameter evenly distributed along the preferential erosion zone, was connected to the DC power supply using an applied power of 1200 W. These holes allow us to control the silver content on the layer by changing the amount of silver pellets (99.9 %) placed in the drilled holes. For this study, four holes were filled with halves of Ag pellets with 10 mm diameter. Finally, for some of the trilayers, a Si_3N_4 layer was deposited on top to serve as a cap layer.

In all the cases, (111) silicon wafers were used as substrates and were submitted to an ultrasonic cleaning procedure in acetone and alcohol for 15 min, prior to the depositions. To increase the adhesion of the trilayers to the substrate, a series of steps were conducted before the final deposition (etching of the substrates and deposition of adhesion interlayers). First, the HiPIMS target (either Ti or Ti target with Si pellets) was cleaned in Ar for 10 min with a discharge pressure of 0.3 Pa. Subsequently, the substrates were ion etched for 30 min, by establishing a pulsed bias of 230 V with a pulsed power supply (ENI RPG-50), while the DC target (Ti with Ag pellets) was cleaned by applying a power of 250 W. After etching, a Ti or TiSi interlayer was produced for 5 min (deposition pressure of 0.3 Pa) with an average power of 1200 W, followed by a gradient layer with increasing N content until the final deposition pressure of 0.7 Pa was reached.

The trilayers were placed in a cylindrical glass tube, which was connected to a vacuum system where the hydrogenated argon was then introduced in the tube (reaching a pressure of 0.1 Pa) to perform the annealing treatments. The specimens were then exposed to a constant linear temperature ramp (from room temperature (RT) up to an isothermal temperature of 600 °C or 800 °C at a rate of 20 °C/min), maintained at these temperatures for 2 h, and then cooled down to RT. The selected isothermal temperatures were selected based on our previous oxidation studies of the TiSiN(Ag) system [39].

After the annealing treatment, lamellas were prepared for TEM analysis by a Focused Ion Beam (FIB) FEI Helios NanoLab 450S Dual-Beam, using gallium ions with an energy of 30 kV. The TEM work was performed in a double-corrector FEI Titan (G3) Cubed Themis. All the observations were performed at 200 kV. High-Angle Annular Dark Field (HAADF) scanning transmission electron microscopy (STEM) images were obtained, coupled with Energy Dispersive Spectroscopy (EDS) analysis to obtain chemical maps and the elemental distribution of the elements. To identify the phases, Selected Area Electron Diffraction

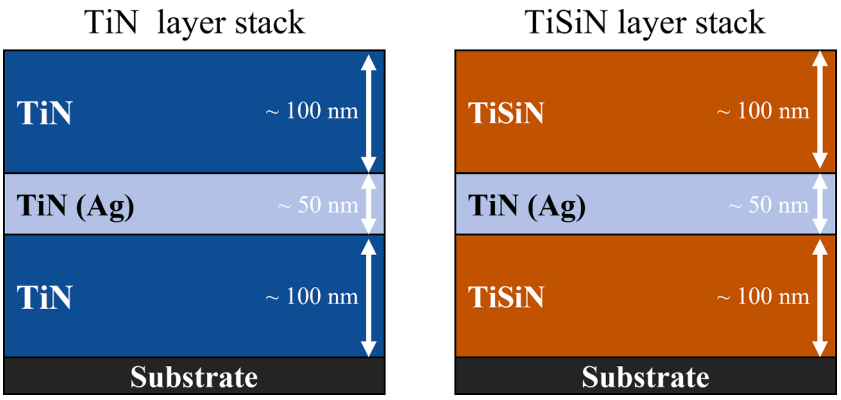

Fig. 1. . Schematic representation of the layer stack coatings studied in this work.

(SAED) patterns were also obtained.

The TEM/STEM experiments were complemented with *in-situ* Rutherford Backscattering Spectrometry (RBS) analysis [41]. RBS samples were heated *in-situ* to 600 and 800 °C in a vacuum atmosphere of 10^{-5} Pa. For each layer stack the following measurements were done: (1) RBS measurements at RT for 30 min, (2) heating to 600 or 800 °C with measurements every minute, (3) isothermal temperature for 2 h with measurements taken every minute and iv) cooling down to RT with continuous 1 min measurements. All the measurements were performed with a 2 MeV He^+ beam. The backscattered ions are detected at a scattering angle of 155° with a solid state detector that is covered with a thin Al layer to make it less sensitive to light produced by the heated sample holder. The beam size was about 3 × 3 mm^2. The RBS spectra were fitted with the program NDF v9.3 g to obtain a model of the sample and elemental concentration depth profiles [42].

3. Results and discussion

3.1. As-deposited trilayers

The cross-section morphology and layer dimensions of the as-deposited trilayers are shown in Fig. 2. Starting with the TiN layer stack (Fig. 2a), it is possible to observe, in the bottom, close to the substrate, the series of interlayers deposited to improve the adhesion of the coatings to the substrate, followed by the bottom TiN layer with a thickness of close to 120 nm. This TiN layer shows a common columnar, although rather dense, morphology. Following this layer, the TiN(Ag) layer with approximately 50 nm is present, where Ag clusters of significantly different sizes, and an agglomeration of clusters, are observed. Finally, the topmost TiN layer with a thickness of close to 120 nm shows a similar columnar morphology, yet the width of the columns increases and the column boundaries are now clearly visible, pointing towards a much less dense and more "open" morphology than the TiN layer at the bottom. This type of morphology can be justified by the presence of the Ag clusters deposited within the "central" layer, which induces a rough surface morphology and, consequently, triggers the atomic shadowing effect [43].

The TiSiN layer stack shows the same architecture as the TiN one. The bottom TiSiN layer displays a columnar but very dense morphology. The central TiN(Ag) layer shows spherical Ag clusters of different sizes. Finally, the top TiSiN layer shows the same tendency as for the TiN layer stack, now much more clearer, exhibiting a much more "open" morphology than its bottom counterpart.

The RBS elemental depth profiles of both as-deposited layer stacks are shown in Fig. 3. The uncertainty in the nitrogen signal is quite large, which is due to the overlapping between nitrogen and silicon (from the substrate) signals in the RBS spectrum. Assuming general values for the density (obtained by taking the weighted mean of the atomic densities), the value of depth of 10^{15} at/cm^2 can be converted to nm and estimated to, roughly, a ratio of 100 × 10^{15} at/cm^2 corresponding to 10 nm. This allows us to confirm and corroborate the thickness of the layers previously measured by TEM (see Fig. 2).

The composition for both the layer stacks can also be estimated using the intensity values for Ti, Si and Ag, having in mind that the nitrogen content should not be considered, due to the uncertainty referred before. In Fig. 3a the composition for the top TiN "sandwich" layer (from 0 × 10^{15} at/cm^2 to 1250 × 10^{15} at/cm^2) showed titanium a little lower than 50 at.%, which was the expected stoichiometry for titanium nitride. The "central" layer (from 1250 × 10^{15} at/cm^2 to 1700 × 10^{15} at/cm^2) shows a value of 20 at.% for Ag and close to 40 at.% for Ti, which corresponds to the expected stoichiometry for TiN. This assumes that silver is not expected to react with nitrogen, due to the very low affinity between these two elements. The interlayer can also be observed, as the value of Ti is now much higher, as expected, since the nitrogen is graded from a specific value down to zero. For the TiSiN layer stack (Fig. 3b), the composition of the top layer (-1050 × 10^{15} at/cm^2) shows Ti and Si values slightly lower than 40, and 10 at.%, respectively, which suggests that the stoichiometry ($TiN + Si_3N_4$) is close to what is expected, noting that, for this case, the (Ti+Si)/N ratio has to be inferior to 1. The interlayer can also be observed for this layer stack; however, as expected, the value for titanium is much lower, as silicon was also being deposited at the same time, which is visible as a shoulder in the Si depth profile (refer to experimental procedure section).

With the morphology of the as-deposited coatings analysed, the layer stacks were subjected to the annealing treatments to assess silver diffusion.

3.2. Silver diffusion at high temperatures

3.2.1. Annealing at 600 °C

The morphology of the, respectively, as-deposited and annealed TiN layer stack and the corresponding mapping of silver after annealing at 600 °C is shown in Fig. 4. As the contrast associated with HAADF STEM is mass-thickness dependant, silver appears brighter in Fig. 4b. By taking a general observation at the morphology of the layer stack it is possible to observe that silver diffusion has occurred at this temperature, as denoted by the brighter contrast observed for the bottom "sandwich" layer when compared to the top "sandwich" layer. To confirm this observation, the elemental map distribution of silver is shown in Fig. 4c, where an intense signal is observed on the "central" layer and a weak

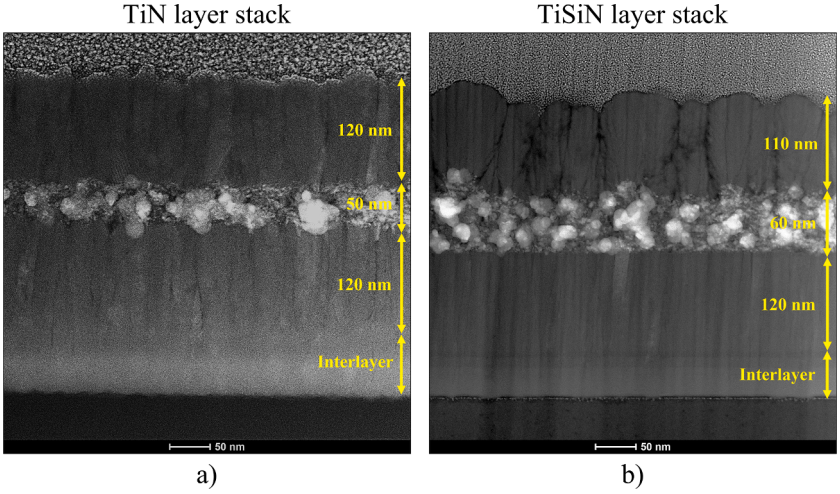

Fig. 2. . Cross-section morphology of the trilayers in the as-deposited state: (a) TiN layer stack and (b) TiSiN layer stack.

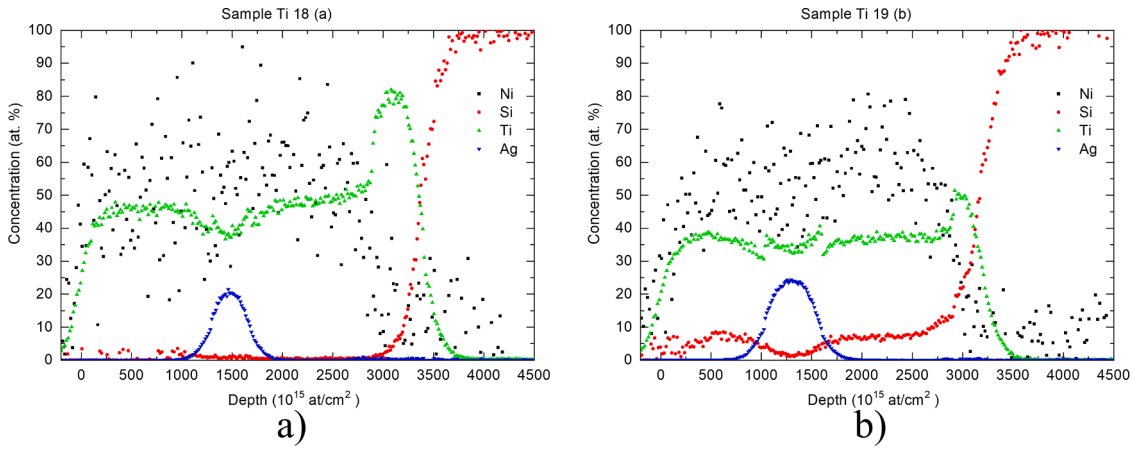

Fig. 3. . RBS elemental concentration depth profiles of the trilayers in the as-deposited state: (a) TiN layer stack and (b) TiSiN layer stack.

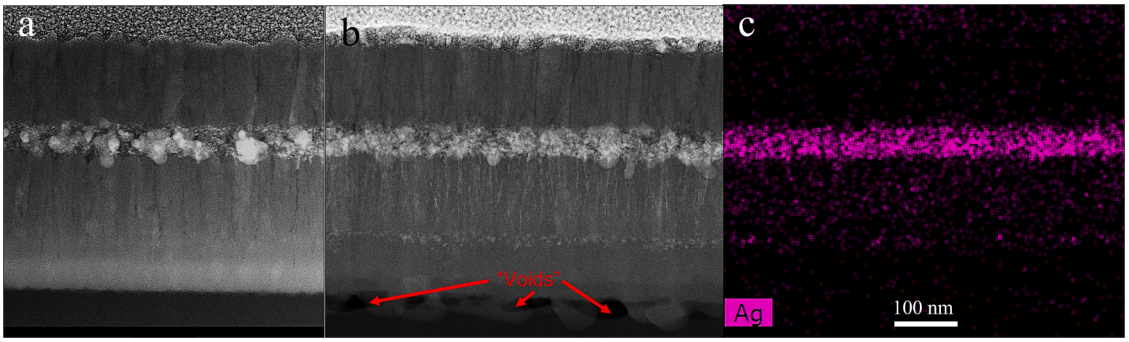

Fig. 4. . (a) As-deposited cross-section HAADF STEM image, (b) annealed cross-section HAADF STEM image and (c) elemental map distribution of silver across the TiN layer stack, after annealing treatment at 600 °C for 2 h.

scattered silver signal is seen on the bottom "sandwich" layer denoting the diffusion of silver into this layer and a slight accumulation at the TiN/adhesion layer interface.

Furthermore, the formation of voids can also be observed in the substrate/interlayer interface (Fig. 4b), which can be explained by the Kirkendall effect [44]. This effect occurs due to the interdiffusion between elements, when sufficient temperature is applied, and one element diffuses much faster, leaving behind some voids. In the case of Ti (interlayer) and Si (substrate), this interdiffusion is reported to occur at temperatures as low as 450 °C with the possible formation of $TiSi_2$ phase at temperatures of 500 °C or higher [45]. As it will be shown later (Section 3.2.2), selected area electron diffraction (SAED) confirms the formation of $TiSi_2$ in this region.

For a very indicative time scale of the Ag redistribution, the RBS spectra of Ag as a function of the annealing time is shown in Fig. 5a. First, note that the three regions plotted represent Ag in the Ag central layer (black colour), Ag diffusing deeper into the sample (blue colour) and Ag diffusing towards the surface (purple colour). It should also be highlighted that Ag in the deepest part of the bottom layer (near the interface with the substrate) cannot be included in the bottom Ag counts

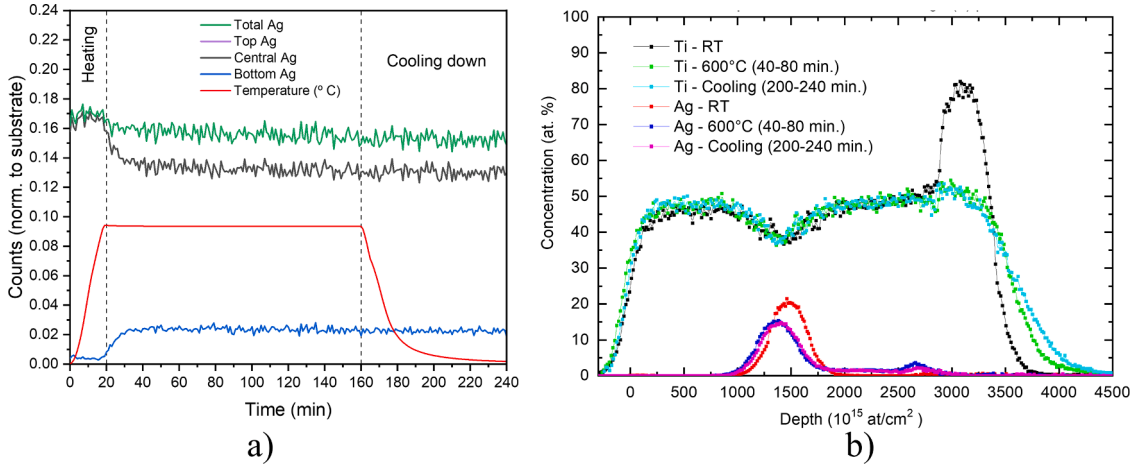

Fig. 5. . RBS results for the TiN layer stack annealed at 600 °C: a) number of Ag counts at various depths in the sample as a function of time and b) depth profiles elemental concentrations of Ti and Ag over the annealing treatment run.

due to overlap in the RBS spectrum. At a first glance, the lack of Top Ag counts is evident as there are no recorded silver in this region. This confirms the observations by TEM (Fig. 4) where elemental maps showed the presence of silver only in the Ag central layer (Central Ag) and towards the interlayer (Bottom Ag). A noticeable gradual increase in the Bottom Ag counts starts close to the 20 min mark (corresponding to the isothermal temperature of 600 °C) and a simultaneous decrease of the Central Ag counts, suggesting the start of the diffusion towards the bottom of the coating. This diffusion seems to occur rapidly in the beginning (until minute 32) and then, halts and remains almost constant for the rest of the experiment. When the cross-section of the film before and after annealing at 600 °C is compared (Fig. 4a and b, respectively), and the tonalities of the different layers analysed, it is clear that the brighter zones (corresponding to the higher atomic number of Ti), become darker due to the incorporation of Si (lower atomic number). In the zone of the gradient layer, it is suggested that the existing low amount of N reacts with Ti forming TiN. Due to the higher density of TiN, in comparison with Ti, small voids can be created at this interface which provides the driving force (concentration diffusion) for diffusing Ag. This process stops when the open spaces are completely filled with Ag, impeding further diffusion of this element. In addition, some diffusion towards the surface might have also occurred since the Total Ag counts are slightly reduced. This fact, combined with the lack of Top Ag counts, suggests that silver diffused to the surface and evaporated/sublimated. This evaporation/sublimation phenomena has been already observed in our previous studies [38,39].

For a better perspective, the elemental depth profiles of Ti and Ag are shown in the RBS spectra shown in Fig. 5b. This allow to confirm that, after the RT period, the Ag signal decreases in the "central" layer over time (at roughly 1300 × 10^{15} at/cm^2) and diffusion occurs towards the interlayer (-2600 × 10^{15} at/cm^2), as corroborated by the increase in Ag signal at this location. Finally, the significant reduction of intensity of the Ti peak at the interface zone, and the broadening of the Ti signal at the interface with the substrate, confirm the intermixing of Ti with silicon from the substrate, due to strong interdiffusion.

Regarding the TiSiN layer stack, the morphology and corresponding elemental map of Ag obtained by cross-sectional TEM analysis are shown in Fig. 6. Contrary to the observations for the TiN layer stack, silver diffusion has not occurred for this layer stack. This suggest that the TiSiN matrix is better in preventing silver diffusion than the TiN matrix. To confirm this, the elemental map distribution clearly displays an intense Ag signal in the "central" layer with no other traces of Ag visible in any other region of the trilayer coating. Just as for the TiN layer stack, the formation of voids at the interlayer/substrate interface also occurs, confirming that the Kirkendall effect is also operational although the amount of interdiffusion is much lower (compare Figs. 5b and 7b for RBS results).

The Ag distribution measured by RBS analysis (Fig. 7a) allows to confirm the aforementioned, with no relevant counts registered for both the Bottom Ag and Top Ag regions corroborating the lack of diffusion observed in the STEM analysis (Fig. 6). However, a slight decrease in the Total Ag is noticed, which might suggest that some silver diffused to the surface and evaporated/sublimated or slightly diffused inwards, since no Top Ag counts were registered. This can be explained by taking into account the difference in the structure of the bottom and the top "sandwich" layers. As discussed before, the morphology of the different layers has an important influence on the diffusion of silver. Thus, a more open structure, facilitates Ag diffusion towards the surface, when compared to the bottom layer, where there is no silver. In any case, the TiSiN matrix still shows a much more promising control of the Ag diffusion than the TiN matrix since this process is still occurring at much lower magnitudes.

Fig. 7b shows that there seems to be an inflection in the Ti profiles around the depths of 1000 × 10^{15} at/cm^2 and 1500 × 10^{15} at/cm^2, which is at the position of the interfaces between the TiSiN and TiN(Ag) layers. This is caused by an error in the calculation of the depth profiles from the RBS spectrum because of a drastic change in the calculated stopping power between the adjacent layers and a limited depth resolution of the detector. As shown before for the Ag distribution spectra (Fig. 7a), the Ag signal after the annealing treatment (purple line in Fig. 7b), decreases slightly with no intensity in any other region, pointing towards the Ag diffusion to the surface and subsequent evaporation. Lastly, there seems to be a clear shift of both the Ti and Ag profiles after the test is initiated which might be connected, as already referred, to the shrinkage in the thickness of the film.

In general, it is possible to assume that the TiSiN matrix is more promising in controlling silver diffusion than the TiN matrix. The morphology of the "sandwich" layers also seems to show an interesting effect on the diffusion process. In the next sub-section analyses of the same layer stacks will be performed after their annealing at higher temperatures.

3.2.2. *Annealing at 800 °C*

The idea of increasing the annealing temperature is to increase the kinetics of mass transport, so that a better understanding of silver diffusion in the different matrixes might be achieved. The temperature of 800 °C has also been used in isothermal studies of TiSiN based films, in our previous work [39], where the absence of Ag outwards diffusion was observed for the non-oxidized film.

The HAADF STEM image and the correspondent elemental map distribution of silver for the TiN layer stack is shown in Fig. 8. When compared with HAADF STEM images obtained at 600 °C (Fig. 4), the contrast suggests that the diffusion of silver to the bottom of the layer stack is strongly increased. However, as the mobility is enhanced at this temperature, the accumulation of silver at the bottom is evident, whereas in the "central" layer, it is now barely present. A clear "intermixing" at the interlayer/substrate interface is again observed. However, the voids are not "visible" as they were for 600 °C. These results can be explained again by the analysis of the possible phases that are being developed at the interface. Although the Ti-Ag phase diagram

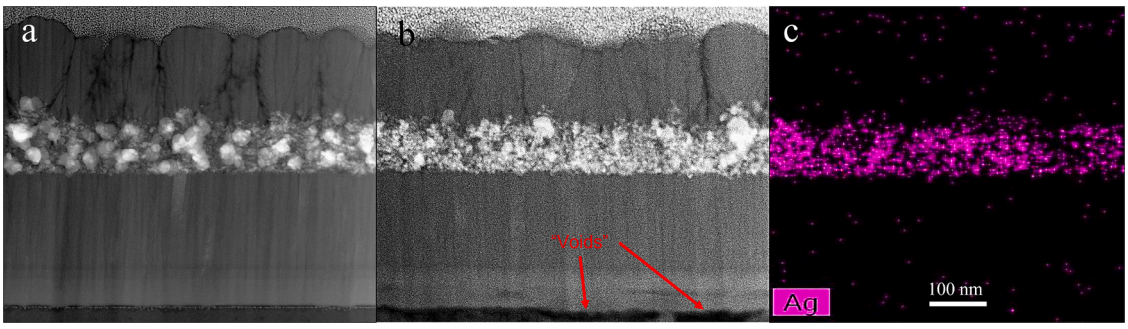

Fig. 6. . (a) As-deposited cross-section HAADF STEM image, b) annealed cross-section HAADF STEM image and c) elemental map distribution of silver across the TiSiN layer stack, after annealing treatment at 600 °C for 2 hours.

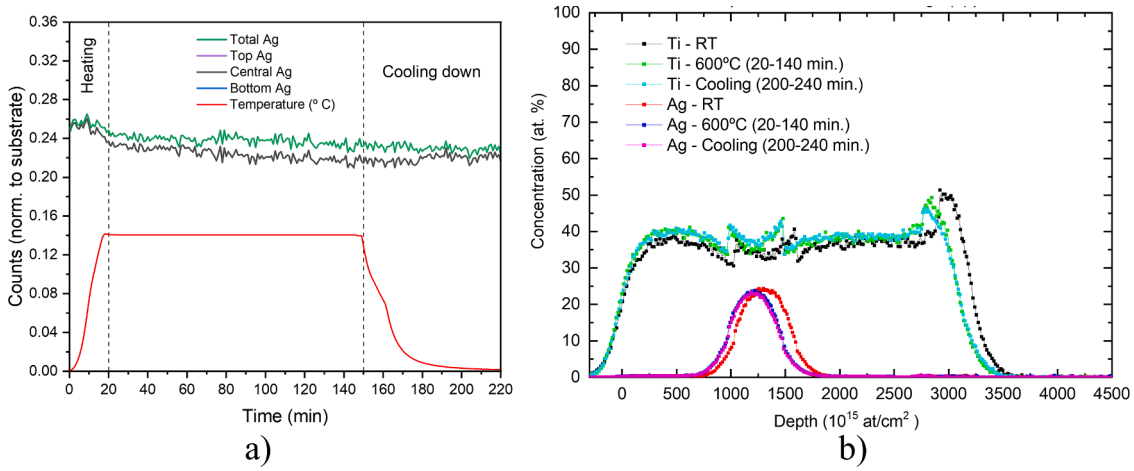

Fig. 7. . RBS results for the TiSiN layer stack annealed at 600 °C: a) number of Ag counts at various depths in the sample as a function of time and b) depth profiles elemental concentrations of Ti and Ag over the annealing treatment run.

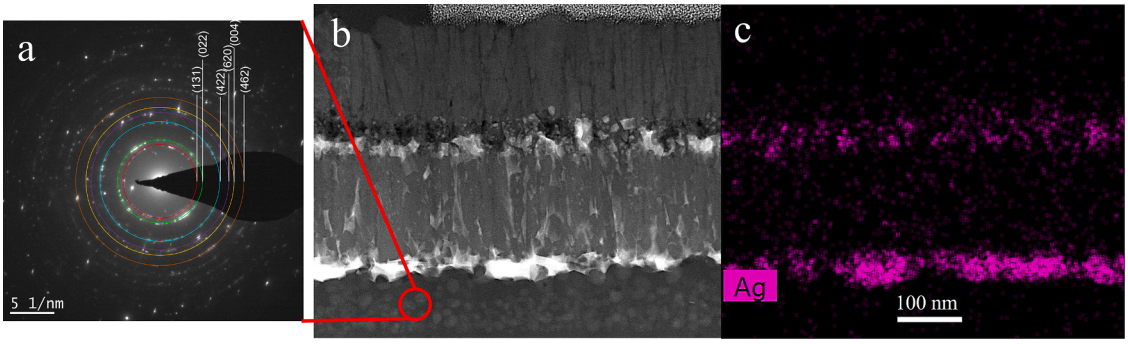

Fig. 8. . a) SAED for the represented area, b) annealed cross-section HAADF STEM image and c) elemental map distribution of silver across the TiN layer stack, after annealing treatment at 800 °C for 2 hours.

predicts the formation of intermetallic TiAg phases [46], we found no evidence of any of these phases. SAED analysis (Fig. 8a) was conducted at the interlayer, in the area represented in Fig. 8b. The electron diffraction suggests the formation of the $TiSi_2$ phase (PDF 00–035–0785) as well as TiN. Elemental distribution maps obtained by EDS support this conclusion (see Fig. 9). Particles of TiN are embedded in a $TiSi_2$ matrix (see superimposition of Ti and N signals for the particles). The precipitation/formation of TiN from the interlayer is clear as well as the crystallization of the $TiSi_2$. As referred in the literature, the interdiffusion process of Ti and Si starts by the formation of an amorphous phase [45] with the crystallization occuring for higher annealing temperatures. As referred to above, the TiN formation occurs with the contraction of the material since TiN is denser than Ti. Again, it's the formation of TiN which allows to create the voids in the interface between the TiN layer and the interlayer promoting the diffusion of Ag from the interface to the bottom of the layer stack. However, there is a counteracting process where an inverse trend should occur, i.e., the crystallization of $TiSi_2$ which, having the lowest density amongst other possible phases, Ti, TiN (4.0 against 4.5 and 5.4 gr/cm^3, respectively), occurs with a strong dilation. This phenomenon will counteract the creation of voids explained before for the 600 °C.

The Ag distribution in the different regions as a function of time for the TiN layer stack is shown on Fig. 10a. It looks like the Ag distribution agrees with the STEM observations (Fig. 8), as shown by an increase in the Bottom Ag counts and a clear decrease in the Central Ag counts. This increase in the Bottom Ag is much smaller than the results obtained by STEM. However, Ag accumulating at the interface with the substrate, as is visible in Fig. 8, is at lower depths then that represented by the Bottom Ag counts and cannot be represented in this way due to overlap in the RBS spectrum. Ag accumulated at the interface can be seen in the depth profile in Fig 10b. But this accumulation is also much smaller than the decrease in the central region. Furthermore, the fact that the Total Ag

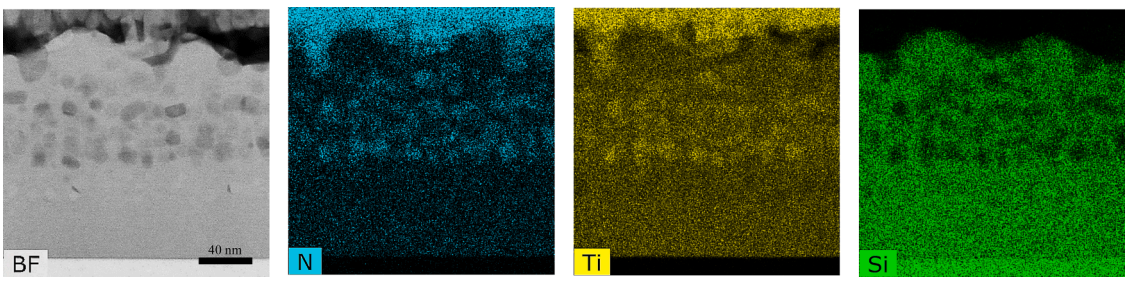

Fig. 9. . Elemental map distribution of the different elements in the bottom interface of the TiN layer stack after annealing treatment at 800 °C for 2 hours.

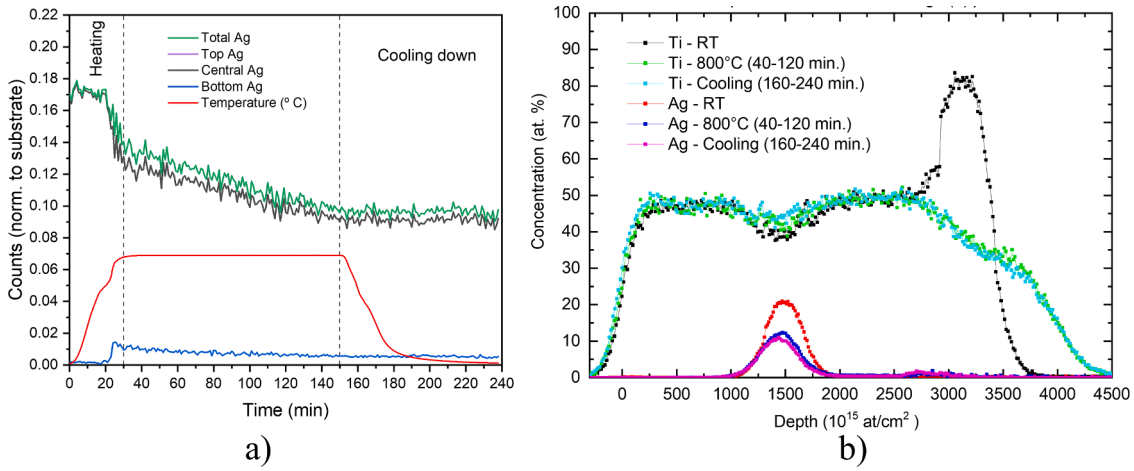

Fig. 10. . RBS results for the TiN layer stack annealed at 800 °C: a) number of Ag counts at various depths in the sample as a function of time and b) depth profiles elemental concentrations of Ti and Ag over the annealing treatment run.

counts are also decreasing at the same rate than the Central Ag, suggests that a large amount of silver diffused to the surface and then evaporated (since no Top Ag counts were registered). This shows that a discrepancy between STEM and RBS results exists since, in the case of STEM observations, silver diffusion to the bottom is most prominent while, in the case of RBS, most of the Ag diffusion occurs to the surface. Nonetheless, the main idea is that Ag diffusion for this matrix occurs relatively easy, as shown by depletion of Ag from the central layer.

The discrepancy between the behaviours of Ag diffusion in the samples analysed by STEM or RBS can be tentatively explained by either the difference in the thermal annealing procedure, or the more open morphology of the top TiN layer comparatively with the bottom one. As described in the experimental section, TEM samples were prepared from layer stacks, which were annealed in an $Ar+H_2$ atmosphere at 10^{-1} Pa whereas RBS samples were vacuum annealed *in situ* at 10^{-5} Pa. As a result, in the case of samples analysed by TEM, annealing at 600 °C and 800 °C promoted the interdiffusion at the interface, structural transformations and the creation of voids (strong vacuum). This favours the Ag diffusion preferentially in relation to the diffusion to the external atmosphere ($Ar+H_2$, 10^{-1} Pa). Moreover, for the case of the samples analysed by RBS at 800 °C, the external atmosphere is at high vacuum, which combined with the more open morphology of the external layer, favours Ag diffusion preferentially outwards than inwards, towards the interlayer.

At 600 °C, the more "open" structure of the top "sandwich" layer provides an easier pathway for Ag diffusion. In fact, although the diffusion of Ag was primarily towards the interlayer, a small amount of Ag also diffused to the surface and sublimated. The HAADF STEM image shown in Fig. 8 also shows that the path for Ag diffusion towards the interlayer, seems to be along the column boundaries. This validates the simulations of Ag diffusion in TiN matrix conducted in a previous work [47] where it was found that Ag could not diffuse through interstitial sites, but should occur on surfaces or grain boundaries.

The elemental depth profiles for Ti and Ag are shown in Fig. 10b, confirming the reduction of silver concentration with the annealing treatment as well as the very weak Ag amount at the interface. As referred to before, in the case of the samples analysed by RBS, the silver is preferentially diffusing to the surface and evaporating. On the other hand, the strong decrease of Ti signal at the interface and the broadening of the peak at the interface confirm the strong intermixing with the silicon from the substrate.

For the TiSiN layer stack, the STEM image and corresponding Ag elemental map distribution is shown in Fig. 11. The STEM images and elemental mapping shows that the silver is completely absent from this layer stack. In addition, as already observed for all the other coatings, the formation of voids due to the Kirkendall effect is quite visible, as the voids are not filled with Ag.

The amount of Ag in the central layer as a function of time is shown in Fig. 12a. The RBS results clearly corroborate the absence of silver with a decrease of the Central Ag counts after the isothermal temperature is reached. This movement of silver seems to occur very fast with the total depletion occurring after around 1 hour. Due to the lack of both Bottom Ag and Top Ag counts it is feasible to assume that silver has diffused rapidly to the surface followed by evaporation, leading to the total absence of Ag.

The immediate analyses of the annealing results of both trilayers,

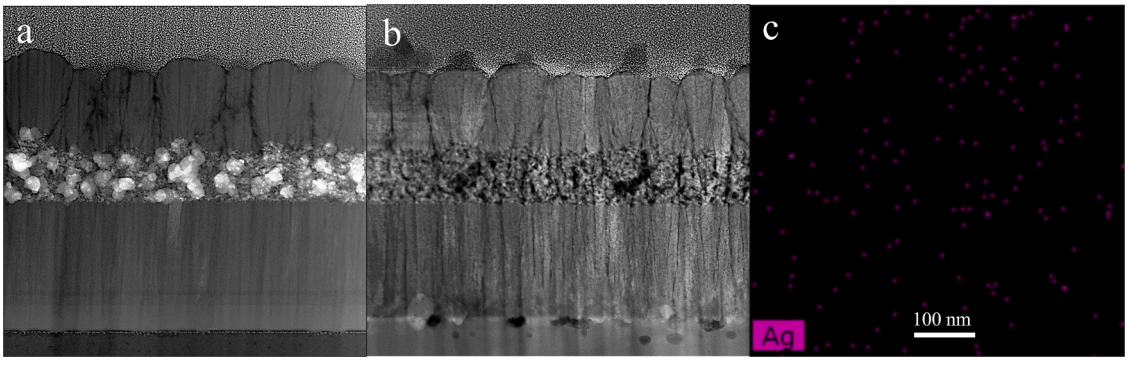

Fig. 11. . (a) As-deposited cross-section HAADF STEM image, (b) annealed cross-section HAADF STEM image and (c) elemental map distribution of silver across the TiSiN layer stack, after annealing treatment at 800 °C for 2 hs.

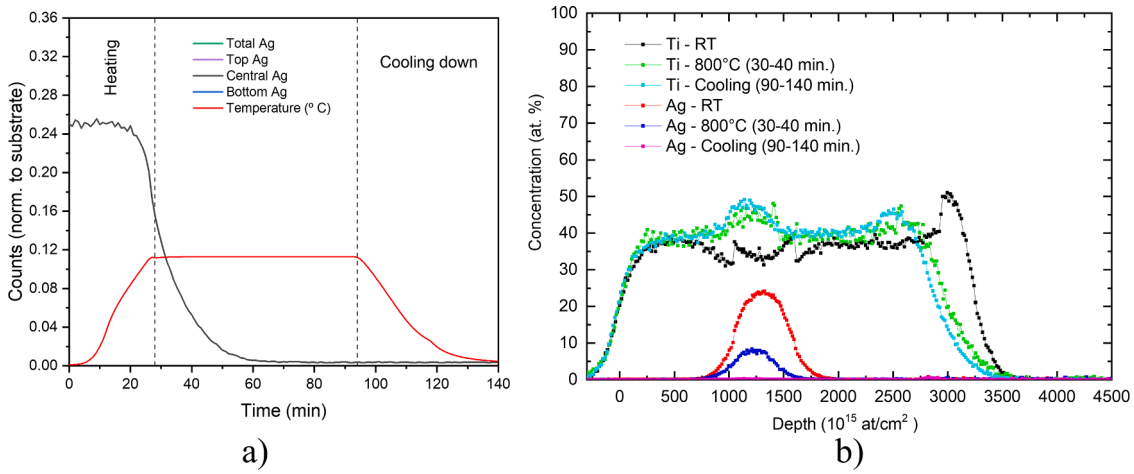

Fig. 12. . RBS results for the TiSiN layer stack annealed at 800 °C: (a) number of Ag counts at various depths in the sample as a function of time and (b) depth profiles elemental concentrations of Ti and Ag over the annealing treatment run.

allows to conclude that the TiN matrix provide a better control of Ag diffusion, than the TiSiN matrix, particularly at 800 °C. In fact, in the case of TiN, some silver still remains in the coating after the annealing. However, if the difference in the morphology of the "sandwich" layers is taken into account as well as the fact that no diffusion was detected to the bottom TiSiN layer (contrarily to what was observed to the TiN), it is feasible to assume that morphology can play a huge role on the control on the diffusion of silver. In this case, the top "sandwich" layer morphology is so "open" (Fig. 11), with much wider columns, that the pathways to diffusion are facilitated. Furthermore, bear in mind that, when the temperature was lower (600 °C), despite the open structure, there was no silver diffusion (see Fig. 6), whereas for the TiN, there was already diffusion towards the surface and towards the bottom of the coating (see Fig. 4). This indicates that silver diffusion, for the case of the TiSiN matrix, requires a much higher driving force (higher temperatures and easier diffusion pathways) to occur.

The elemental depth profiles for the Ti and Ag in the TiSiN layer stack are shown in Fig. 12b. The Ag profiles confirm that silver is diffusing and vanishing from the coating with the concentration clearly decreasing as the annealing is occurring (blue line in Fig. 12b). As a result, no relevant counts are detected for silver at the bottom or the surface of the coating. The titanium profiles show an increase in the atomic concentration in the layer that contained Ag, as the annealing process is occurring. As can be observed, this zone is shrinking with the annealing time, therefore increasing the total Ti content to values higher than the ones existing in the sandwich layer (these contain Si). The creation of voids also results in the shrinking of the layer in units of at/cm^2 (as used in the figure).

To summarize, it seems that the TiSiN matrix is not so efficient in controlling the Ag diffusion as the TiN matrix. However, by combining the results observed at 600 °C and 800 °C with the morphology of the "sandwich" layers, it is reasonable to assume that the TiSiN matrix requires a much stronger driving force for the diffusion process to occur than the TiN matrix. To confirm and corroborate this hypothesis, Si_3N_4 cap layers were deposited on top of both layer stacks and then subjected to another annealing process (600 °C and 800 °C) to clarify the role of the morphology in Ag diffusion.

3.2.3. *Application of Si_3N_4 cap layers*

STEM images of the layer stacks with the cap layer subjected to annealing treatment are shown in Fig. 13. The TiN layer stack annealed at 600 °C (Fig. 13a) shows the diffusion of silver to the "bottom" sandwich layer, as shown before (Fig. 4). Moreover, with the cap layer, it is now possible to confirm that the Ag also diffuses to the surface, as shown by its accumulation at the "top" sandwich layer. A similar behaviour occurs for the same type of layer stack annealed at 800 °C, where there is a significant silver diffusion to the "bottom" sandwich layer, mimicking the image of the correspondent sample without the cap layer (see Fig. 8). Finally, the TiSiN layer stack annealed at 600 °C shows no migration of silver, similar to what was observed in the sample without cap layer

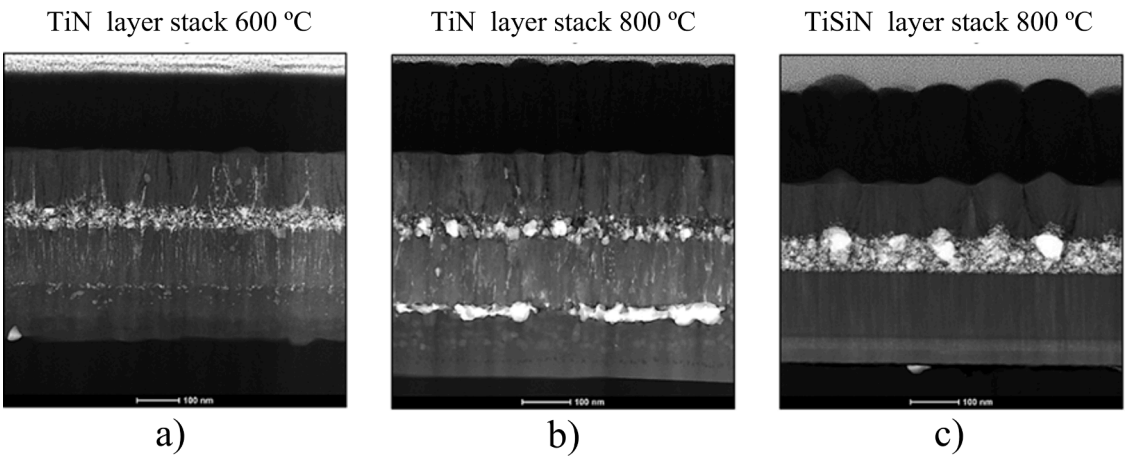

Fig. 13. . TEM micrographs of the trilayers with the Si_3N_4 cap layer: (a) TiN layer stack annealed at 600 °C, (b) TiN layer stack annealed at 800 °C and (c) TiSiN layer stack annealed at 600 °C.

(Fig. 6) where outwards diffusion to the surface was hypothesized. For all of these coatings, the interdiffusion in the interface film / substrate can be observed.

At 800 °C, instead of the complete disappearance of silver observed for the TiSiN layer stack (see Fig. 11), the cap layer allows to conclude that a complete "stop" of silver diffusion is possible (see Fig. 14a). The elemental map distribution (Fig. 14b) shows that all the silver is concentrated in the initial "central" layer. TiSiN then shows that, depending on the morphology, is a matrix that requires a much higher driving force to initiate the diffusion process in comparison to the TiN matrix. This confirms what was observed in our previous study of this system [38,39] where similar compact structure was able to be achieved all throughout and diffusion was found to be stagnant.

4. Conclusions

Silver diffusion in TiN and TiSiN triple layer stacks was studied in order to identify the preconditions for an optimal, slow release of the noble metal dry lubricant. The stacks were comprised of a central Ag-rich layer (in a TiN matrix) sandwiched between two layers of the same matrix (in this case, either TiN or TiSiN). In order to simulate the conditions of dry machining, the samples were subjected to annealing treatments at 600 °C and 800 °C for 2 hours. The morphology and the Ag-distribution in the as-deposited and annealed stacks were analysed by element specific transmission electron microscopy techniques. Rutherford backscattering spectrometry was employed to monitor the element depth distribution *in situ*, i.e., in real time during the annealing treatment and, to quantify the Ag redistribution processes.

The TEM analysis revealed a columnar morphology of all as-deposited coatings, but with a different degree of compactness. Soon it was realised that this difference in the morphology of the triple layers would have an impact in the Ag diffusion degree during the annealing treatments.

After subjecting the coatings to annealing treatments at 600 °C, silver diffusion towards the interface between the "bottom" stack layer and the Ti-rich adhesion layer was observed for the TiN layer stack. This diffusion path is attributed to the creation of small voids in the interface between the bottom coating of the layer stack and the interlayer, resulting from the formation of TiN. In contrast to that, the dense morphology of TiSiN prevented this type of Ag diffusion in the other layer stack. This observation indicated that the TiSiN matrix could be more promising for controlling the Ag diffusion. In addition to inward diffusion, Ag diffusion to the surface and subsequent evaporation/sublimation was observed for both matrices. The total loss of Ag by this diffusion path was the same for both matrices (TiN: 17 at.% –> 15.5 at.% and TiSiN: 26 at.% –> 24 at.%; the relative loss is 9 % and 8%), reflecting that the upper layers of both stacks had a similar, more open morphology.

For the increased annealing temperature, the TiN layer stack showed qualitatively the same behaviour as for the 600 °C treatment. However, the amount of Ag-loss was higher than for the annealing at 600 °C, and less Ag was found at the bottom interface. This showed the preference for outward diffusion and sublimation since the temperature of 800 °C is close to the melting point of the metal. This effect was even more pronounced for the TiSiN stack, for which no Ag was found anymore by both analysis techniques after the annealing at 800 °C due to the missing diffusion path towards the inner interface.

The application of cap layers on top of the stacks prevented the sublimation-driven path of Ag diffusion. Moreover, it confirmed the successful suppression of the inwards diffusion of the metal due to the dense morphology of the bottom TiSiN layer. Our study shows that the silver diffusion in hard coatings can be controlled by applying matrices which enable slow release of the noble-metal-based dry lubricant to the surface and prevent diffusion towards inner interfaces. The TiSiN coating studied here is a promising candidate for achieving this effect in dry-machining applications.

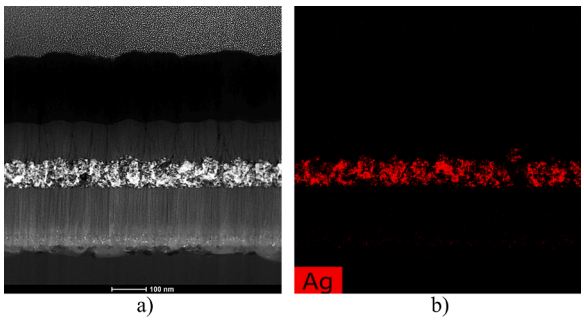

Fig. 14. . (a) Cross-section HAADF STEM micrograph, (b) elemental map distribution of silver of the TiSiN layer stack with the Si_3N_4 cap layer after annealing treatment at 800 °C for 2 h.

Author statement

The authors declare that they revised and replied to all the questions and comments placed by the reviewers, to the best of our knowledge. The authors also declare that a manuscript with the highlighted changes was also supplied during the review process.

The authors would also like to thank the editor and the reviewers for their suggestions and/or comments that can help with improving the manuscript.

CRediT authorship contribution statement

D. Cavaleiro: Writing – original draft, Investigation, Visualization, Methodology. **F. Munnik:** Validation, Investigation, Formal analysis, Data curation, Writing – review & editing. **M. Krause:** Methodology, Formal analysis, Data curation, Writing – review & editing. **E. Carbo-Argibay:** Methodology, Investigation, Visualization, Data curation. **P.J. Ferreira:** Methodology, Formal analysis, Investigation, Writing – review & editing. **A. Cavaleiro:** Conceptualization, Methodology, Formal analysis, Writing – review & editing, Funding acquisition. **F. Fernandes:** Conceptualization, Formal analysis, Writing – review & editing, Project administration, Funding acquisition.

Declaration of Competing Interest

The authors declare the following financial interests/personal relationships which may be considered as potential competing interests: Filipe Fernandes reports financial support was provided by Foundation for Science and Technology.

Data availability

Data will be made available on request.

Acknowledgments

This research is sponsored by FEDER funds through the program COMPETE – Programa Operacional Factores de Competitividade – and by national funds through FCT – Fundação para a Ciência e a Tecnologia –, under the projects: MCTool21 - ref. "POCI-01–0247- FEDER-045940″, CEMMPRE – ref. "UIDB/00285/2020″ and ARISE - ref. "LA/P/0112/2020". This work was also supported by FCT, through IDMEC, under LAETA, project UIDB/50022/2020 and by project number 19001567-ST-1.1-IBC at the Institute of Ion Beam Physics and Materials Research – HZDR.

References

[1] Energy information administration, *Annual energy review*, acessed October 2022, https://www.eia.gov/totalenergy/data/annual/index.php.
[2] T. Herzog, World Greenhouse Gas Emissions in 2005, World Resources Institute, 2009.
[3] N.A. Abukhshim, P.T. Mativenga, M.A. Sheikh, Heat generation and temperature prediction in metal cutting: a review and implications for high speed machining, Int. J. Mach. Tools Manuf. 46 (2006) 782–800.
[4] T.G. Gutowski, M.S. Branham, J.B. Dahmus, A.J. Jones, A. Thiriez, D.P. Sekulic, Thermodynamic analysis of resources used in manufacturing processes, Environ. Sci. Technol. 43 (2009) 1584–1590.
[5] G.S. Goindi, P. Sarkar, Dry machining: a step towards sustainable machining – challenges and future directions, J. Cleaner Prod. 165 (2017) 1557–1571.
[6] N. Khanna, J.P. Davim, Design-of-experiments application in machining titanium alloys for aerospace structural components, Measurement 61 (2015) 280–290.
[7] M. Kuttolamadom, J. Jones, L. Mears, T. Kurfess, A. Choragudi, Investigation of the Machining of Titanium Components For Lightweight Vehicles, SAE International, 2010.
[8] A. Pramanik, Problems and solutions in machining of titanium alloys, Int. J. Adv. Manuf. Technol. 70 (2014) 919–928.
[9] E.O. Ezugwu, Z.M. Wang, Titanium alloys and their machinability—a review, J. Mater. Process. Technol. 68 (1997) 262–274.
[10] R. M'Saoubi, D. Axinte, S.L. Soo, C. Nobel, H. Attia, G. Kappmeyer, S. Engin, W. M. Sim, High performance cutting of advanced aerospace alloys and composite materials, CIRP Ann. 64 (2015) 557–580.
[11] S. Zhang, W. Zhu, TiN coating of tool steels: a review, J. Mater. Process. Technol. 39 (1993) 165–177.
[12] S. Carvalho, N.M.G. Parreira, M.Z. Silva, A. Cavaleiro, L. Rebouta, In-service behaviour of (Ti,Si,Al)Nx nanocomposite films, Wear 274-275 (2012) 68–74.
[13] A. Biksa, K. Yamamoto, G. Dosbaeva, S.C. Veldhuis, G.S. Fox-Rabinovich, A. Elfizy, T. Wagg, L.S. Shuster, Wear behavior of adaptive nano-multilayered AlTiN/MexN PVD coatings during machining of aerospace alloys, Tribol. Int. 43 (2010) 1491–1499.
[14] A. Erdemir, B. Bhushan, Solid lubricants and self-lubricating films. Modern Tribology Handbook, CRC Press, 2001, pp. 787–825.
[15] A.A. Voevodin, C. Muratore, S.M. Aouadi, Hard coatings with high temperature adaptive lubrication and contact thermal management: review, Surf. Coat. Technol. 257 (2014) 247–265.
[16] F. Gustavsson, S. Jacobson, A. Cavaleiro, T. Polcar, Ultra-low friction W–S–N solid lubricant coating, Surf. Coat. Technol. 232 (2013) 541–548.
[17] M.A. Hamilton, L.A. Alvarez, N.A. Mauntler, N. Argibay, R. Colbert, D.L. Burris, C. Muratore, A.A. Voevodin, S.S. Perry, W.G. Sawyer, A possible link between macroscopic wear and temperature dependent friction behaviors of MoS2 coatings, Tribol. Lett. 32 (2008) 91–98.
[18] M.R. Hilton, R. Bauer, P.D. Fleischauer, Tribological performance and deformation of sputter-deposited MoS2 solid lubricant films during sliding wear and indentation contact, Thin. Solid. Films 188 (1990) 219–236.
[19] J.J. Hu, J.E. Bultman, C. Muratore, B.S. Phillips, J.S. Zabinski, A.A. Voevodin, Tribological properties of pulsed laser deposited Mo–S–Te composite films at moderate high temperatures, Surf. Coat. Technol. 203 (2009) 2322–2327.
[20] S.M. Aouadi, H. Gao, A. Martini, T.W. Scharf, C. Muratore, Lubricious oxide coatings for extreme temperature applications: a review, Surf. Coat. Technol. 257 (2014) 266–277.
[21] A. Magneli, Structures of the ReO3-type with recurrent dislocations of atoms: `homologous series' of molybdenum and tungsten oxides, Acta Crystallogr. 6 (1953) 495–500.
[22] J.S. Zabinski, J.H. Sanders, J. Nainaparampil, S.V. Prasad, Lubrication using a microstructurally engineered oxide: performance and mechanisms, Tribol. Lett. 8 (2000) 103–116.
[23] J.J. Hu, C. Muratore, A.A. Voevodin, Silver diffusion and high-temperature lubrication mechanisms of YSZ–Ag–Mo based nanocomposite coatings, Compos. Sci. Technol. 67 (2007) 336–347.
[24] H.E. Sliney, The use of silver in self-lubricating coatings for extreme temperatures, A S L E Trans. 29 (1986) 370–376.
[25] A.A. Voevodin, J.J. Hu, J.G. Jones, T.A. Fitz, J.S. Zabinski, Growth and structural characterization of yttria-stabilized zirconia–gold nanocomposite films with improved toughness, Thin Solid Films 401 (2001) 187–195.
[26] F.P. Bowden, F.P. Bowden, D. Tabor, The Friction and Lubrication of Solids, Oxford university press, 2001.
[27] S.C Velasco, A. Cavaleiro, S. Carvalho, Functional properties of ceramic-Ag nanocomposite coatings produced by magnetron sputtering, Prog. Mater. Sci. 84 (2016) 158–191.
[28] C. Wang, X. Yu, M. Hua, Microstructure and mechanical properties of Ag-containing diamond-like carbon films in mid-frequency dual-magnetron sputtering, Appl. Surf. Sci. 256 (2009) 1431–1435.
[29] C.C. Tseng, J.H. Hsieh, W. Wu, S.Y. Chang, C.L. Chang, Emergence of Ag particles and their effects on the mechanical properties of TaN–Ag nanocomposite thin films, Surf. Coat. Technol. 201 (2007) 9565–9570.
[30] C.P. Mulligan, T.A. Blanchet, D. Gall, CrN–Ag nanocomposite coatings: High-temperature tribological response, Wear, 269 (2010) 125–131.
[31] C.P. Mulligan, D. Gall, CrN–Ag self-lubricating hard coatings, Surf. Coat. Technol. 200 (2005) 1495–1500.
[32] C. Muratore, A.A. Voevodin, J.J. Hu, J.S. Zabinski, Tribology of adaptive nanocomposite yttria-stabilized zirconia coatings containing silver and molybdenum from 25 to 700°C, Wear 261 (2006) 797–805.
[33] D.S. Stone, S. Harbin, H. Mohseni, J.E. Mogonye, T.W. Scharf, C. Muratore, A. A. Voevodin, A. Martini, S.M. Aouadi, Lubricious silver tantalate films for extreme temperature applications, Surf. Coat. Technol. 217 (2013) 140–146.
[34] P.A. Papi, C.P. Mulligan, D. Gall, CrN–Ag nanocomposite coatings: control of lubricant transport by diffusion barriers, Thin Solid Films 524 (2012) 211–217.
[35] C. Muratore, A.A. Voevodin, J.J. Hu, J.S. Zabinski, Multilayered YSZ–Ag–Mo/TiN adaptive tribological nanocomposite coatings, Tribol. Lett. 24 (2006) 201–206.
[36] S. Vepřek, S. Reiprich, A concept for the design of novel superhard coatings, Thin Solid Films 268 (1995) 64–71.
[37] G. Bilger, T. Voss, T. Schlenker, A. Strohm, High-temperature diffusion barriers from Si-rich silicon-nitride, Surf. Interface Anal. 38 (2006) 1687–1691.
[38] D. Cavaleiro, S. Carvalho, A. Cavaleiro, F. Fernandes, TiSiN(Ag) films deposited by HiPIMS working in DOMS mode: Effect of Ag content on structure, mechanical properties and thermal stability, Appl. Surf. Sci. (2019).
[39] D. Cavaleiro, A. Cavaleiro, S. Carvalho, F. Fernandes, Oxidation behaviour of TiSiN (Ag) films deposited by high power impulse magnetron sputtering, Thin Solid Films 688 (2019), 137423.
[40] D. Cavaleiro, D. Figueiredo, C.W. Moura, A. Cavaleiro, S. Carvalho, F. Fernandes, Machining performance of TiSiN(Ag) coated tools during dry turning of TiAl6V4 aerospace alloy, Ceram. Int. 47 (2021) 11799–11806.
[41] R. Wenisch, F. Lungwitz, D. Hanf, R. Heller, J. Zscharschuch, R. Hübner, J. von Borany, G. Abrasonis, S. Gemming, R. Escobar-Galindo, M. Krause, Cluster tool for *in situ* processing and comprehensive characterization of thin films at high temperatures, Anal. Chem. 90 (2018) 7837–7842.
[42] N.P. Barradas, C. Jeynes, R.P. Webb, Simulated annealing analysis of Rutherford backscattering data, Appl. Phys. Lett. 71 (1997) 291–293.
[43] F. Fernandes, S. Calderon V, P.J. Ferreira, A. Cavaleiro, J.C. Oliveira, Low peak power deposition regime in HiPIMS: deposition of hard and dense nanocomposite Ti-Si-N films by DOMS without the need of energetic bombardment, Surf. Coat. Technol. 397 (2020), 125996.
[44] X. Zhao, L. Duan, Y. Wang, Fast interdiffusion and Kirkendall effects of SiC-coated C/SiC composites joined by a Ti-Nb-Ti interlayer via spark plasma sintering, J. Eur. Ceram. Soc. 39 (2019) 1757–1765.
[45] I.J.M.M. Raaijmakers, A.H. Reader, P.H. Oosting, The formation of an amorphous silicide by thermal reaction of sputter-deposited Ti and Si layers, J. Appl. Phys. 63 (1988) 2790–2795.
[46] O. Dezellus, R. Arroyave, S.G. Fries, Thermodynamic modelling of the Ag–Cu–Ti ternary system, Int. J. Mater. Res. 102 (2011) 286–297.
[47] V. Lenzi, A. Cavaleiro, F. Fernandes, L. Marques, Diffusion of silver in titanium nitride: Insights from density functional theory and molecular dynamics, Appl. Surf. Sci. 556 (2021), 149738.